



## Measurement of $B_s^0 \rightarrow D_s^{(*)+} D_s^{(*)-}$ Branching Ratios

The CDF Collaboration  
URL <http://www-cdf.fnal.gov>  
(Dated: March 1, 2012)

The decays  $B_s^0 \rightarrow D_s^{(*)+} D_s^{(*)-}$  are reconstructed in a data sample corresponding to an integrated luminosity of  $6.8 \text{ fb}^{-1}$  collected by the CDF II detector at the Tevatron  $p\bar{p}$  collider. We measure the  $B_s^0$  production rate times  $B_s^0 \rightarrow D_s^{(*)+} D_s^{(*)-}$  branching ratios relative to the normalization mode  $B^0 \rightarrow D_s^+ D^-$  to be  $0.183 \pm 0.021 \pm 0.017$  for  $B_s^0 \rightarrow D_s^+ D_s^-$ ,  $0.424 \pm 0.046 \pm 0.035$  for  $B_s^0 \rightarrow D_s^{*\pm} D_s^{\mp}$ ,  $0.654 \pm 0.072 \pm 0.065$  for  $B_s^0 \rightarrow D_s^{*+} D_s^{*-}$ , and  $1.261 \pm 0.095 \pm 0.112$  for the inclusive decay  $B_s^0 \rightarrow D_s^{(*)+} D_s^{(*)-}$ , where the uncertainties are statistical and systematic. These results are the most precise single measurements to date and provide important constraints for indirect searches for non-standard model physics in  $B_s^0$  mixing.

## I. INTRODUCTION

A  $B_s^0$  meson can oscillate into its antiparticle via second order weak interaction transitions, which make its time evolution sensitive to contributions from new physics processes. Such contributions are not well constrained yet and might be responsible for the deviation from the standard model reported in Ref. [1]. The  $B_s^0$  eigenstates with defined mass and lifetime,  $B_{sL}^0$  and  $B_{sH}^0$ , are linear combinations of the  $B_s^0$  and  $\bar{B}_s^0$  states and, in the standard model, correspond in good approximation to the even and odd  $CP$  eigenstates, respectively. In the absence of substantial  $CP$  violation, a sizable decay width difference between the light and heavy mass eigenstates,  $\Delta\Gamma_s = \Gamma_{sL} - \Gamma_{sH}$ , arises from the fact that decays to final states of definite  $CP$  are only accessible by one of the mass eigenstates. The dominant contribution to  $\Delta\Gamma_s$  is believed to come from the  $B_s^0 \rightarrow D_s^{(*)+} D_s^{(*)-}$  decays [2], which are predominantly  $CP$ -even and saturate  $\Delta\Gamma_s$  under certain theoretical assumptions [3, 4], resulting in the relation

$$2\mathcal{B}(B_s^0 \rightarrow D_s^{(*)+} D_s^{(*)-}) \approx \frac{\Delta\Gamma_s}{\Gamma_s + \Delta\Gamma_s/2}, \quad (1)$$

where  $\Gamma_s = (\Gamma_{sL} + \Gamma_{sH})/2$  [5]. However, three-body modes may provide a significant contribution to  $\Delta\Gamma_s$  [6].

A finite value of  $\Delta\Gamma_s$  improves the experimental sensitivity to  $CP$  violation because it allows one to distinguish the two mass eigenstates via their decay time distribution. Furthermore, the  $B_s^0 \rightarrow D_s^{(*)+} D_s^{(*)-}$  decays could be used in future to measure directly the lifetime of the  $CP$ -even eigenstate, which would complement the  $CP$ -odd eigenstate lifetime measurement in  $B_s^0 \rightarrow J/\psi f_0(980)$  decays [7] and provide additional information in the search for new physics contributions to  $CP$  violation in the  $B_s^0$  system.

The  $B_s^0 \rightarrow D_s^{(*)+} D_s^{(*)-}$  decay modes have been previously studied by the ALEPH, CDF, D0, and Belle collaborations [8–11]. The current world average branching ratios [12], which do not yet include the latest preliminary Belle results [13], are  $\mathcal{B}(B_s^0 \rightarrow D_s^+ D_s^-) = (1.04_{-0.26}^{+0.29})\%$ ,  $\mathcal{B}(B_s^0 \rightarrow D_s^{\pm} D_s^{\mp}) = (2.8 \pm 1.0)\%$ ,  $\mathcal{B}(B_s^0 \rightarrow D_s^{*+} D_s^{*-}) = (3.1 \pm 1.4)\%$ , and  $\mathcal{B}(B_s^0 \rightarrow D_s^{(*)+} D_s^{(*)-}) = (4.5 \pm 1.4)\%$ .

In a data sample corresponding to an integrated luminosity of  $6.8 \text{ fb}^{-1}$  recorded by the CDF II detector at the Tevatron  $p\bar{p}$  collider we reconstruct  $B_s^0 \rightarrow D_s^{(*)+} D_s^{(*)-}$  decays with  $D_s^+ \rightarrow K^+ K^- \pi^+$ . For the first time in this channel, the acceptance is calculated using a  $D_s^{\pm}$  Dalitz model instead of a simple two-body decay model. The photon and the neutral pion from the  $D_s^{*+} \rightarrow D_s^+ \gamma$  and  $D_s^{*+} \rightarrow D_s^+ \pi^0$  decays are not reconstructed because of their low detection efficiency. In a simultaneous fit to the reconstructed  $B_{(s)}^0$  meson invariant mass spectra we measure the  $B_s^0$  production rate times  $B_s^0 \rightarrow D_s^{(*)+} D_s^{(*)-}$  branching ratios relative to the normalization mode  $B^0 \rightarrow D_s^+ D^-$

$$f_X = \frac{f_s}{f_d} \frac{\mathcal{B}(B_s^0 \rightarrow X)}{\mathcal{B}(B^0 \rightarrow D_s^+ D^-)}, \quad (2)$$

for  $X = D_s^+ D_s^-, D_s^{*\pm} D_s^{\mp}, D_s^{*+} D_s^{*-}$ , and the inclusive  $D_s^{(*)+} D_s^{(*)-}$  where  $f_s/f_d$  is the relative rate of produced  $B_s^0$  to  $B^0$  mesons.

## II. CDF II DETECTOR

The components of the CDF II detector [14] most relevant for this analysis are the tracking systems located inside a solenoid that provides a 1.4 T magnetic field. Charged particles' trajectories (tracks) are reconstructed in layers of silicon-strip sensors located between radii of 1.5 cm and 28 cm from the beam line and an open-cell drift chamber (COT) with a radial extension from 40 to 137 cm. Tracks with a pseudorapidity  $|\eta| \leq 1.0$  pass the full radial extent of the COT. Kaons and pions are statistically identified by measurements of the ionization energy loss in the COT and information from the time-of-flight system located between the COT and the solenoid. The events for this analysis are selected online by identifying pairs of tracks detected in the COT and the silicon detector [15]. Minimal requirements on the momenta and the displacement of the tracks and the reconstructed decay vertex from the primary vertex are imposed.

## III. RECONSTRUCTION AND SELECTION

We reconstruct  $D_s^+ \rightarrow K^+ K^- \pi^+$  and  $D^+ \rightarrow K^- \pi^+ \pi^+$  decays from combinations of three tracks with appropriate charge and mass hypothesis assignments, fitted to a common vertex. Because the  $D_s^+ \rightarrow K^+ K^- \pi^+$  decay proceeds mainly via  $\phi\pi^+$  and  $\bar{K}^{*0}K^+$ , we select candidates with  $1.005 < m(K^+ K^-) < 1.035 \text{ GeV}/c^2$  and  $0.837 < m(K^- \pi^+) <$

0.947 GeV/ $c^2$ , centered on the known  $\phi$  and  $K^{*0}$  masses, respectively. According to the  $D_s^+ \rightarrow K^+K^-\pi^+$  Dalitz structure [16] this requirement has a signal acceptance of about 75% while covering only 14% of the phase space and thus increasing the signal-to-background ratio. In the following we will denote the selected  $K^+K^-$  and  $K^-\pi^+$  combinations as  $\phi$  and  $\bar{K}^{*0}$ , respectively, since the dominant contributions come from these resonances. However, we implicitly include contributions from other resonances and interference effects when using these terms.

Pairs of  $D_s^+ \rightarrow \phi\pi^+$  or  $D_s^+ \rightarrow \bar{K}^{*0}K^+$  candidates and  $D_s^- \rightarrow \phi\pi^-$  candidates are combined to form  $B_s^0$  candidates and fitted to a common vertex. Combinations where both charm mesons decay into a  $\bar{K}^{*0}$  mode are not considered because of the low signal-to-background ratio. Candidate  $B^0$  mesons are reconstructed from  $D_s^+D^-$  combinations where both  $D_s^+$  decay modes are used.

To reject background-like events, requirements are placed on track quality variables,  $B$  meson momentum, reconstructed  $D$  meson masses, vertex fit qualities, and vertex displacement significances. To further increase the signal purity, two artificial neural networks are used, one for candidates with a  $\bar{K}^{*0}$  and one for candidates without. To minimize the systematic uncertainty of the relative selection efficiency, the same networks are applied to  $B_s^0$  and  $B^0$  candidates, and only information from the  $D_s^\pm$  that is common to both  $B$  meson decays is used. The networks are trained on simulated signal events, described below, and on background events from the 5.45 to 6.5 GeV/ $c^2$   $B$  mass sideband. The input variables contain kinematic, lifetime, fit quality, and particle identification information. The  $B$  vertex displacement significance in the transverse plane gives the largest contribution to the discrimination power of both networks. The selection criteria on the network outputs are chosen such that they maximize the significance  $\epsilon_{\text{MC}}/\sqrt{N_{\text{data}}}$ , where  $\epsilon_{\text{MC}}$  is the  $B_s^0$  selection efficiency determined from simulation and  $N_{\text{data}}$  is the number of data events in the  $B_s^0$  signal window from 5.343 to 5.397 GeV/ $c^2$ .

About 6% of the selected  $B^0 \rightarrow D_s^+(\rightarrow \phi\pi^+)D^-$  candidates also fulfill the  $B_s^0$  selection requirements, where the assignment of a  $D^-$  daughter track is swapped from pion to kaon. To avoid having the same event entering the fit multiple times, we reject each event that is reconstructed as  $B_s^0$  candidates from the  $B^0$  sample. The cross-populations between the two  $B_s^0$  modes and between the two  $B^0$  modes, respectively, are negligible. The selected sample contains about 750  $B_s^0$  signal events.

#### IV. SIMULATION

Simulated events are used to determine the reconstruction and selection efficiency. The  $B_{(s)}^0$  mesons are generated according to the momentum spectrum measured in exclusive  $B$  decays and decayed to the considered final states with the EVTGEN package [17]. For the  $B_s^0$  meson we assign the lifetime of the  $B_{sL}^0$  eigenstate [12] that coincides with the  $CP$ -even eigenstate in the standard model. For all the other long-lived charm and bottom mesons, the world average mean lifetimes [12] are used. The  $B_s^0 \rightarrow D_s^{*+}D_s^{*-}$  decay is a transition of a scalar to two vector mesons and its angular distribution is described by three polarization amplitudes. Since these amplitudes are unknown, we take the same longitudinal polarization as measured in  $B^0 \rightarrow D^{*+}D^{*-}$  decays [18] and a vanishing  $CP$ -odd component as default values. The world average value [12] is used for the ratio of  $D_s^{*+} \rightarrow D_s^+\gamma$  to  $D_s^{*+} \rightarrow D_s^+\pi^0$  decays. The dynamics of the decay  $D_s^+ \rightarrow K^+K^-\pi^+$  is simulated according to the Dalitz structure measured by CLEO [16]. The generated events are processed by a GEANT3 based detector simulation [19] and the same reconstruction program as applied to real data events.

#### V. FIT

The relative branching ratios times production rate are determined in a simultaneous extended unbinned maximum-likelihood fit to the  $(\phi\pi^+)(\phi\pi^-)$ ,  $(\bar{K}^{*0}K^+)(\phi\pi^-)$ ,  $(\phi\pi^+)(K^+\pi^-\pi^-)$ , and  $(\bar{K}^{*0}K^+)(K^+\pi^-\pi^-)$  invariant mass distributions. By simultaneously fitting all four distributions, the normalization of the  $B^0$  reflections in the  $(\bar{K}^{*0}K^+)(\phi\pi^-)$  spectrum is constrained by the yields in the high-statistics  $(\phi\pi^+)(K^+\pi^-\pi^-)$  sample. The components of the fit function for each invariant mass distribution are fully and partially reconstructed signals, reflections, and background. The fully reconstructed  $B_s^0$  and  $B^0$  signals are parametrized by the sum of two Gaussians with relative normalizations and widths derived from simulation. To account for discrepancies between data and simulation, a factor is introduced for the  $B_s^0$  and  $B^0$  signal shapes, respectively, that scales the widths of the Gaussians and that is allowed to float in the fit. The shapes of partially reconstructed signal events and of reflections from  $B^0 \rightarrow (\phi\pi^+)(K^+\pi^-\pi^-)$  misreconstructed as  $B_s^0 \rightarrow (\phi\pi^+)(K^{*0}K^-)$  are determined from simulation using empirical models. Background from random combinations of tracks and other  $B$  decays is described by an exponential plus a constant function with all parameters floated in the fit.

The yield of fully reconstructed  $B^0$  mesons in the final state  $i$ ,  $(\phi\pi^+)(K^+\pi^-\pi^-)$  or  $(\bar{K}^{*0}K^+)(K^+\pi^-\pi^-)$ , is given

by

$$N_{\text{rec},i}^{B^0} = N_{\text{tot}}^{B^0} \mathcal{B}(B^0 \rightarrow D_s^+ D^-) \mathcal{B}(D_s^+ \rightarrow K^+ K^- \pi^+) \mathcal{B}(D^+ \rightarrow K^- \pi^+ \pi^+) \epsilon_i^{B^0}, \quad (3)$$

where  $N_{\text{tot}}^{B^0}$  is the total number of produced  $B^0$  mesons and is a free parameter in the fit, the branching ratios are taken from Ref. [12], and the efficiency  $\epsilon_i^{B^0}$  is determined from simulation. Equivalent expressions are used for the yields of partially reconstructed  $B^0$  decays with an additional branching ratio factor for the  $D^{*+}$  and  $D_s^{*+}$  decays. The normalizations of reflections are calculated in the same way, but with the efficiencies replaced by the mis-reconstruction fractions determined from simulation. The number of fully reconstructed  $B_s^0$  mesons in the final state  $i$ ,  $(\phi\pi^+)(\phi\pi^-)$  or  $(\bar{K}^{*0}K^+)(\phi\pi^-)$ , where the  $D_s^+$  decays in the same mode as the  $D_s^+$  from the  $B^0$  decay is given by

$$N_{\text{rec},i}^{B_s^0} = N_{\text{rec},i}^{B^0} f_{D_s D_s} \frac{\mathcal{B}(D_s^+ \rightarrow K^+ K^- \pi^+) \epsilon_i^{B_s^0}}{\mathcal{B}(D^+ \rightarrow K^- \pi^+ \pi^+) \epsilon_i^{B^0}}, \quad (4)$$

with  $f_{D_s D_s}$  as a free parameter and  $N_{\text{rec},i}^{B^0}$  given by Eq. (3). Equivalent equations hold for partially reconstructed  $B_s^0$  decays.

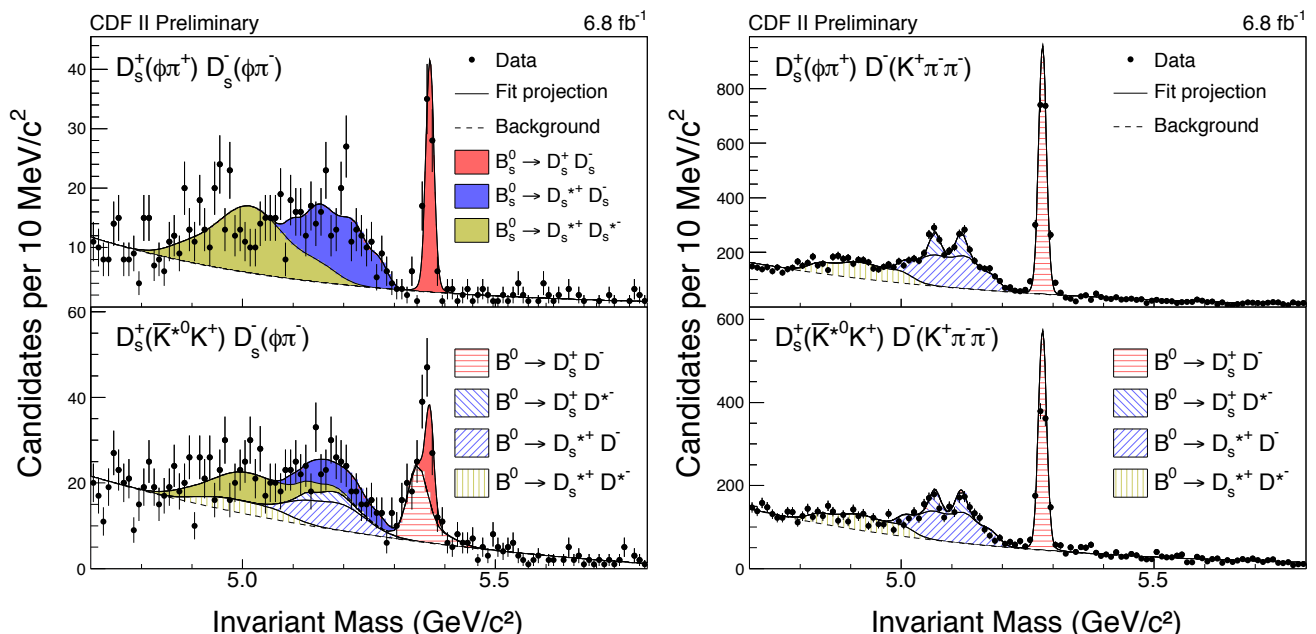


FIG. 1. Invariant mass distribution of  $B_s^0 \rightarrow D_s^+(\phi\pi^+)D_s^-(\phi\pi^-)$ ,  $B_s^0 \rightarrow D_s^+(\bar{K}^{*0}K^+)D_s^-(\phi\pi^-)$ ,  $B^0 \rightarrow D_s^+(\phi\pi^+)D^-(K^+\pi^-\pi^-)$ , and  $B^0 \rightarrow D_s^+(\bar{K}^{*0}K^+)D^-(K^+\pi^-\pi^-)$  candidates with the simultaneous fit projection overlaid. The broader structures stem from decays where the photon or  $\pi^0$  from the  $D_{(s)}^+$  decay is not reconstructed. Misreconstructed  $B^0$  signal events show up as reflections in the lower left plot.

Projections of the fit result are compared to the distribution of data events in Fig. 1. The statistical significance of each signal exceeds  $10\sigma$  as estimated from a likelihood ratio of the fit with and without the signal component.

## VI. SYSTEMATIC UNCERTAINTIES

Systematic uncertainties on the fitted signal yields arise from the signal and background models. Because the width scale factors of the fully reconstructed signal components are allowed to float in the fit, the systematic uncertainties of these components are already included in the statistical errors. To estimate the systematic effect due to the fixed shapes of the partially reconstructed signal components and reflections, we repeat the fit multiple times with shape parameters randomly varied according to the covariance matrix of the fits of the shapes to simulated data. The mean deviations with respect to the central values are assigned as systematic uncertainties. The systematic uncertainties due to the background mass model are estimated from the changes in the results caused by using a second order

Source	$f_{D_s D_s}$	$f_{D_s^* D_s}$	$f_{D_s^* D_s^*}$	$f_{D_s^{(*)} D_s^{(*)}}$
Signal model	0.003	0.007	0.009	0.019
Background model	0.001	0.004	0.030	0.033
Detector simulation	0.001	0.003	0.010	0.005
$B, D$ lifetimes	+0.001 -0.002	+0.002 -0.004	+0.003 -0.006	+0.006 -0.012
Dalitz model	0.011	0.024	0.038	0.073
Helicity model	0.001	0.005	0.012	0.008
Branching fractions	0.013	0.024	0.039	0.074
Total	0.017	0.035	0.065	0.112

TABLE I. Overview of systematic uncertainties on the measured ratios of branching fractions.

polynomial instead of the sum of an exponential and a constant function. By applying the selection optimization procedure on the normalization instead of the signal mode we verified that a possible selection bias is negligible.

Systematic effects in the relative efficiency determination can be caused by a simulation that does not describe the data accurately. One source of systematic uncertainties is the trigger simulation, which can lead to a discrepancy in the  $B$  meson momentum spectrum. Although this effect cancels to first order in the ratio measurement, it is accounted for by a reweighting of the simulated events. The systematic uncertainties due to the detector simulation are estimated by the shift of the results with respect to the case in which this reweighting is not applied. The uncertainties on the world average  $B^0$ ,  $D^+$ , and  $D_s^+$  lifetimes are propagated by varying the lifetimes in the simulation. For the  $B_s^0$  lifetime, we consider two cases, the  $1\sigma$  lower bound of the world average short-lived eigenstate lifetime and the  $1\sigma$  upper bound of the mean  $B_s^0$  lifetime. The effects on the acceptance induced by variations of the  $D_s^+ \rightarrow K^+ K^- \pi^+$  Dalitz structure are considered by generating different Dalitz model scenarios, with Dalitz model parameter values varied according to the systematic and correlated statistical uncertainties of the CLEO Dalitz fit. The uncertainties of the  $D^+$  Dalitz model have a negligible effect on the result. For  $B_s^0 \rightarrow D_s^{*+} D_s^{*-}$  decays we investigate the effects of both a longitudinal polarization fraction  $f_L$  deviating from our nominal assumption and a non-zero fraction of the  $CP$ -odd component  $f_{CP-}$ . The fraction  $f_L$  is varied in the simulation according to the uncertainty of the  $f_L$  measurement in  $B^0 \rightarrow D^{*+} D^{*-}$  decays [18]. A variation of  $f_{CP-}$  shows no effect on the  $B_s^0 \rightarrow D_s^{*+} D_s^{*-}$  mass line shape, fit quality, or measured branching fraction ratios. The effect of self cross-feed due to a wrong assignment of kaon and pion masses is negligible.

Further systematic uncertainties arise from external input quantities. The uncertainties of intermediate and final state branching fractions,  $\mathcal{B}(D_s^+ \rightarrow K^+ K^- \pi^+)$ ,  $\mathcal{B}(D^+ \rightarrow K^- \pi^+ \pi^+)$ , and  $\mathcal{B}(D^{*+} \rightarrow D^+ \gamma / \pi^0)$ , are propagated in the fit by adding Gaussian constraints to the corresponding fit parameters. The resulting uncertainties of the measured branching fraction ratios are extracted by subtracting in quadrature the statistical uncertainties of the fits with branching fraction constrained and the one where they are fixed to the central values. When calculating the absolute branching fractions  $\mathcal{B}(B_s^0 \rightarrow D_s^{(*)+} D_s^{(*)-})$  an additional relative uncertainty of 16% is introduced by the measurement uncertainties of  $f_s/f_d$  and the branching fraction of the normalization channel  $B^0 \rightarrow D_s^+ D^-$ . The systematic uncertainties are summarized in Table I.

## VII. RESULT

As a result we obtain  $f_{D_s D_s} = 0.183 \pm 0.021 \pm 0.017$ ,  $f_{D_s^* D_s} = 0.424 \pm 0.046 \pm 0.035$ ,  $f_{D_s^* D_s^*} = 0.654 \pm 0.072 \pm 0.065$ , and  $f_{D_s^{(*)} D_s^{(*)}} = 1.261 \pm 0.095 \pm 0.112$ , where the first uncertainties are statistical and the second systematic. Taking  $\mathcal{B}(B^0 \rightarrow D_s^+ D^-) = (7.2 \pm 0.8) \times 10^{-3}$  from Ref. [12] and  $f_s/f_d = 0.269 \pm 0.033$  from Ref. [12, 20] an absolute inclusive branching ratio of  $\mathcal{B}(B_s^0 \rightarrow D_s^{(*)+} D_s^{(*)-}) = (3.38 \pm 0.25 \pm 0.30 \pm 0.56)\%$  is calculated where the third uncertainty comes from the normalization. Assuming Eq. (1) to hold this would translate into a decay width difference contribution of the  $B_s^0 \rightarrow D_s^{(*)+} D_s^{(*)-}$  modes of  $\Delta\Gamma_s/\Gamma_s = (6.99 \pm 0.54 \pm 0.64 \pm 1.20)\%$ .

## VIII. CONCLUSION

In summary, we have measured the branching ratios of  $B_s^0 \rightarrow D_s^+ D_s^-$ ,  $B_s^0 \rightarrow D_s^{\pm} D_s^{\mp}$ ,  $B_s^0 \rightarrow D_s^{*+} D_s^{*-}$ , and  $B_s^0 \rightarrow D_s^{(*)+} D_s^{(*)-}$  decays relative to the normalization mode  $B^0 \rightarrow D_s^+ D^-$ . Compared to previous analyses, we have reduced the systematic uncertainties by taking into account the full  $D_s^+ \rightarrow K^+ K^- \pi^+$  Dalitz structure, as opposed to using a simple two-body  $D_s^+$  decay model. The derived absolute branching ratios of  $\mathcal{B}(B_s^0 \rightarrow D_s^+ D_s^-) = (0.49 \pm 0.06 \pm$

$0.05 \pm 0.08$  %,  $\mathcal{B}(B_s^0 \rightarrow D_s^{*\pm} D_s^{\mp}) = (1.13 \pm 0.12 \pm 0.09 \pm 0.19)$  %,  $\mathcal{B}(B_s^0 \rightarrow D_s^{*+} D_s^{*-}) = (1.75 \pm 0.19 \pm 0.17 \pm 0.29)$  %, and  $\mathcal{B}(B_s^0 \rightarrow D_s^{(*)+} D_s^{(*)-}) = (3.38 \pm 0.25 \pm 0.30 \pm 0.56)$  %, where the uncertainties are statistical, systematic, and due to the normalization, are the most precise measurements to date. The central values are lower than but consistent with the Belle result [11] and the previous CDF result.

### ACKNOWLEDGMENTS

We thank Mikhail S. Dubrovin and David Cinabro for their help in implementing the CLEO Dalitz model. We thank the Fermilab staff and the technical staffs of the participating institutions for their vital contributions. This work was supported by the U.S. Department of Energy and National Science Foundation; the Italian Istituto Nazionale di Fisica Nucleare; the Ministry of Education, Culture, Sports, Science and Technology of Japan; the Natural Sciences and Engineering Research Council of Canada; the National Science Council of the Republic of China; the Swiss National Science Foundation; the A.P. Sloan Foundation; the Bundesministerium für Bildung und Forschung, Germany; the Korean World Class University Program, the National Research Foundation of Korea; the Science and Technology Facilities Council and the Royal Society, UK; the Russian Foundation for Basic Research; the Ministerio de Ciencia e Innovación, and Programa Consolider-Ingenio 2010, Spain; the Slovak R&D Agency; the Academy of Finland; and the Australian Research Council (ARC).

- 
- [1] V. M. Abazov *et al.* (D0 Collaboration), Phys. Rev. D **84**, 052007 (2011).
  - [2] Charge-conjugate modes are implicitly included throughout this paper.
  - [3] R. Aleksan *et al.*, Phys. Lett. B **316**, 567 (1993).
  - [4] M. A. Shifman and M. B. Voloshin, Yad. Fiz. **47**, 801 (1988) [Sov. J. Nucl. Phys. **47**, 511 (1988)].
  - [5] I. Dunietz, R. Fleischer and U. Nierste, Phys. Rev. D **63**, 114015 (2001).
  - [6] C. K. Chua, W. S. Hou, and C. H. Shen, Phys. Rev. D **84**, 074037 (2011).
  - [7] T. Aaltonen *et al.* (CDF Collaboration), Phys. Rev. D **84**, 052012 (2011).
  - [8] R. Barate *et al.* (ALEPH Collaboration), Phys. Lett. B **486**, 286 (2000).
  - [9] T. Aaltonen *et al.* (CDF Collaboration), Phys. Rev. Lett. **100**, 021803 (2008).
  - [10] V. M. Abazov *et al.* (D0 Collaboration), Phys. Rev. Lett. **102**, 091801 (2009).
  - [11] S. Esen *et al.* (Belle Collaboration), Phys. Rev. Lett. **105**, 201802 (2010).
  - [12] K. Nakamura *et al.* (Particle Data Group), J. Phys. G **37**, 075021 (2010), and 2011 partial update.
  - [13] S. Esen, arXiv:hep-ex/1110.2099.
  - [14] D. E. Acosta *et al.* (CDF Collaboration), Phys. Rev. D **71**, 032001 (2005).
  - [15] E. J. Thomson *et al.*, IEEE Trans. Nucl. Sci., **49**, 1063 (2002); B. Ashmanskas *et al.*, Nucl. Instrum. Methods A **518**, 532 (2004); L. Ristori and G. Punzi, Ann. Rev. Nucl. Part. Sci **60**, 595 (2010).
  - [16] R. E. Mitchell *et al.* (CLEO Collaboration), Phys. Rev. D **79**, 072008 (2009).
  - [17] D. Lange, Nucl. Instrum. Methods A **462**, 152 (2001).
  - [18] B. Aubert *et al.* (BaBar Collaboration), Phys. Rev. D **67**, 092003 (2003).
  - [19] R. Brun, R. Hagelberg, M. Hansroul, and J. Lassalle, CERN-DD-78-2-REV, 1978 (unpublished).
  - [20] T. Aaltonen *et al.* (CDF Collaboration), Phys. Rev. D **77**, 072003 (2008).